

ELECTRON-BEAM-DRIVEN RI SEPARATOR FOR SCRIT AT RIKEN RI BEAM FACTORY

T. Ohnishi*, S. Ichikawa, and M. Wakasugi

RIKEN Nishina Center for Accelerator-Based Science, Wako, Saitama, Japan

Abstract

Electron-beam-driven RI separator for SCRIT (ERIS) was constructed for the SCRIT (Self-Confinement RI Target) electron scattering facility at RIKEN RI Beam Factory. It is employed to produce low-energy, high-quality, and high-intensity RI beams used for the electron scattering of unstable nuclei. For RI production, ERIS uses the photofission of uranium driven by an electron beam, and the estimated production rate of fission products is 2.2×10^{11} fissions/s with 30-g uranium and a 1-kW electron beam. The RI production in ERIS was started at 2013. After several improvements of production target and ion source, the rate of ^{132}Sn was achieved to 2.6×10^5 atoms/s with 15-g uranium and a 10-W electron beam. Further studies in ERIS are in progress to supply intense RI beams stably for the electron scattering with RI.

INTRODUCTION

Electron scattering is an unambiguous probing method to study the nuclear structure because of the well-known interaction and no internal structure of electron [1]. Thus, electron scattering has been applied to the study of stable nuclei for many years. As for short-lived unstable nuclei, it has not been applied due to the difficulty of preparing unstable nuclei target. To overcome this problem and realize electron scattering of short-lived nuclei, a novel target forming technique, named as SCRIT (Self-Confinement RI Target) [2], was proposed. SCRIT harnesses the ion trapping phenomenon in an electron storage ring. The validity and performance of SCRIT was already demonstrated [3,4]. Based on this successful achievement, the SCRIT electron scattering facility [5] was constructed at RIKEN RI Beam factory, and it has been operated from 2009.

Electron-beam-driven RI separator for SCRIT (ERIS) [6] is constructed as an online isotope separator (ISOL) system which is dedicated to produce a radioactive isotope (RI) beam for the SCRIT facility. In ERIS, the photofission of uranium driven by the electron beam is used for the RI production, because this reaction is effective for producing more neutron-rich isotopes around the tin region compared with other fission reactions [7]. This region is the first target of our project, and ^{132}Sn , especially, is an important nucleus in the study of unstable nuclei owing to its double magic number structure. After the commissioning of the beam line of ERIS, the RI production was started from 2013, and ^{132}Sn was clearly observed in the first attempt [6].

In this paper, we introduce ERIS briefly, and report the recent progress of the production target and the RI production.

EXPERIMENTAL SETUP OF ERIS

Figure 1 shows the schematic layout of ERIS. ERIS consists of a production target, a forced electron beam induced arc discharge (FEBIAD) type ion source, and a beam analyzing transport line. Produced RIs are transported to the SCRIT device installed inside the electron storage ring. Details of the components of ERIS and the result of the commissioning are described in Ref. [6].

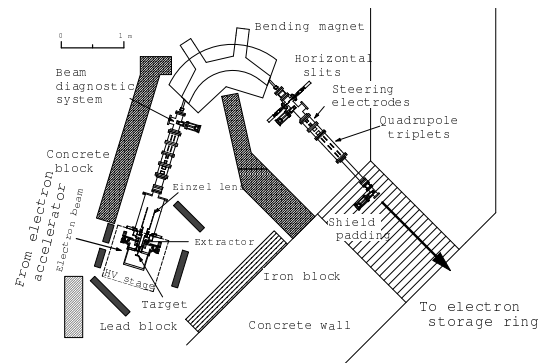


Figure 1: Schematic layout of ERIS. ERIS is surrounded with a concrete wall 2 m in thickness and local shields in the form of concrete, iron, and lead blocks are also installed.

The production target is installed inside a graphite container, which is 21 mm in inner diameter and 60 mm in inner length. This container is surrounded with a tantalum heater, and it is connected to the ion source by the transfer tube. For fast effusion and diffusion, all components are heated up to around 2000 °C. Figure 2 shows a tantalum heater and its setting.

In ERIS, the FEBIAD type ion source is used, because of its applicability to a wide range of elements and its stable operability with high ionization efficiency. The basic design of the ion source is based on CERN ISOLDE [8] and HRIBF [9] at Oak Ridge National Laboratory. Details of the ion source including the electrical connections is described in Ref [6]. This ion source is placed on a high-voltage stage (<50kV) for acceleration.

The beam transport line consists of an einzel lens, a doublet and a triplet electrostatic quadrupoles, four steering electrodes, and a 120° bending magnet with radius of 0.8 m. The diameters of the apertures of the einzel lens and the quadrupole electrodes are 120 and 40 mm, respectively. The maximum magnetic rigidity of the bending magnet is

* oonishi@ribf.riken.jp

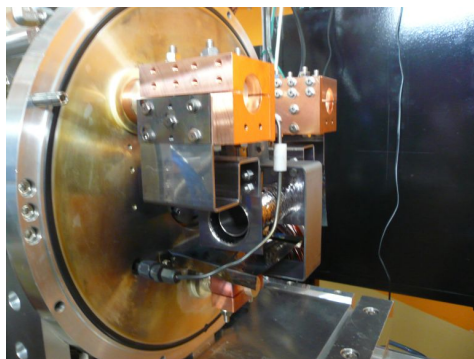


Figure 2: Photograph of tantalum heater and its setting. Cu blocks are heater electrodes connected with tantalum heaters. A thin tube which is connected to transfer tube is a gas inlet.

0.96 Tm. As a result of the commissioning, the mass resolution ($M/\Delta M$) was obtained as about 1600 in σ .

The particle identification system consists of a rotating disk and a Ge detector, and it is installed at the exit of ERIS. The RI beam is stopped inside the rotating disk, and it is moved to the front of the Ge detector. The identification of the stopped RI is performed if specific γ rays corresponding to the decay of the stopped RIs are detected.

The total rate of fission products is estimated from the γ -ray production rate obtained from a Monte Carlo simulation and the measured cross section of the photofission of uranium [10]. In the calculation, a UC_2 target is used, and its density is set to 4.8 g/cm^3 . With 60-mm thick target and 1-kW electron beam, the total fission products is estimated to be 2×10^{11} fissions/s. The production rate of ^{132}Sn is estimated to be 2×10^9 particles/s from the independent chain yield (1%) [11].

PREPARATION OF PRODUCTION TARGET

As a production target, we prepared thin uranium-carbide disks for several merits.: 1) Using a thin target disk, such as 1-mm disk, the efficiency of release from the target is expected to be improved, because the total surface area of target disks becomes large. 2) Uranium carbide is more suitable for production target than uranium oxide, because its vapor pressure and density are lower and higher than those of uranium oxide, respectively. 3) With small amount of oxygen, damages to the material of ion source can be reduced.

Uranium carbide is obtained by the carbothermal reduction of uranium oxide in presence of carbon around 1100–1600°C [12]. First, uranyl nitrate solution was mixed with $20\mu\text{m}$ graphite grains. After the oxidization under air flow at 500°C, uranium-oxide-coated graphite powders were obtained. Next, these powders were manually ground, and formed into a disk without a binder at 180-MPa compression. The formed disk was 20 mm in a diameter and around 1 mm in a thickness, shown in Fig. 3. Finally, uranium-

oxide-coated graphite disk was converted into uranium carbide disk at around 1100–1600°C. The obtained disk was 18 mm in a diameter and 0.8 mm in a thickness. In total, 23 disks were prepared. Total amount of uranium was about 15 g, and the average mass concentration of uranium in the disk was estimated as 3.4 g/cm^3 .



Figure 3: Photograph of 1-mm uranium-oxide-coated target disks. These disks are 20 mm in a diameter and 1 mm in a thickness.

RI PRODUCTION AT ERIS

The prepared uranium-carbide disks were irradiated with an electron beam accelerated to 150 MeV. The maximum electron beam power was nearly 10 W. During the measurement, the electron beam power was adjusted to keep the acceptable counting rate of the detector. Total amount of uranium was about 15 g using 23 prepared thin uranium carbide disks. Tantalum disks with a thickness of 5 mm and a diameter of 20 mm were inserted in front of the production target to increase the production of γ rays. The temperature of the target and the transfer tube was approximately 2000°C. Produced RIs were accelerated to 20 kV and mass-separated by the beam transport line of ERIS. They were identified by the particle identification system.

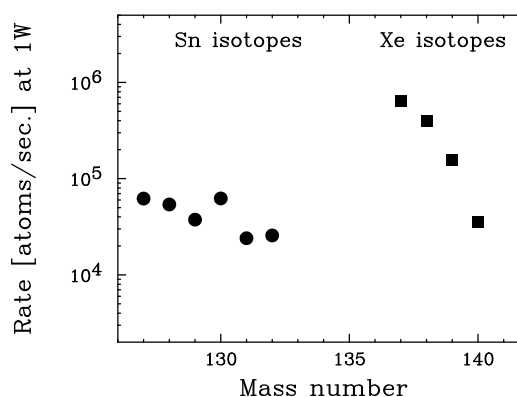


Figure 4: Rate of Sn and Xe isotopes at the particle identification detector at ERIS. Total amount of uranium is 15 g. The electron beam power is normalized to 1 W.

Figure 4 shows the rate of tin and xenon isotopes at the Ge detector. These rates are estimated from the observed γ -ray yield using the efficiency of the Ge detector and the

half-life of each isotope. These rates are normalized using the measured electron beam power. The overall efficiency is the ratio of the observed rate to the expected production rate inside the target. This efficiency includes the efficiency of release from the target, ionization in the ion source, and efficiency of transport from the ion source to the detector. The overall efficiency of stable xenon with a calibrated gas flow was also measured during the experiment. Since stable xenon was introduced into the ionization chamber through a gas inlet, the measured overall efficiency of stable xenon includes only ionization and transport efficiencies. In the case of tin isotopes, the same ionization and transport efficiency as those of xenon can be used, which is supported by the results at ALTO [13]. As a result, the release efficiency of xenon and tin isotopes can be estimated. Table 1 shows the summary of rate and efficiency in the case of ^{137}Xe and ^{132}Sn . The expected rate is calculated with the measured target density.

Table 1: Summary of Rate and Efficiency with 1-W Beam

	^{137}Xe	^{132}Sn
Observed rate (atoms/sec)	6.4×10^5	2.6×10^4
Expected rate (atoms/sec)	7.5×10^6	1.3×10^6
Overall efficiency	8.4%	2.1%
Overall efficiency of stable xenon	14%	15%
Release efficiency	61%	14%

The release efficiency includes the decay inside the target during the release process and the absorption in the target and the transport line. For ^{132}Sn , the reason of the low release efficiency is considered as the long time for effusion and diffusion due to its chemical property. In order to improve the release efficiency, it is needed to develop the porous structure target and achieve the better thermal uniformity in the transport line.

The stability of the production target at high temperature was also examined measuring the time dependence of the release efficiency. During the measurement period, the temperature of the production target was kept over 2000°C and the irradiation of the electron beam was only performed during the measurement of the efficiency. After 120 hours from the first measurement, the power of the target heater was increased from 4.4 kW to 5 kW. This was corresponding to almost 50 degree temperature rise around 2000°C .

Figure 5 shows the time dependence of the release efficiency of ^{130}Sn and ^{132}Sn . After about 4 days, the release efficiency becomes half of the values at the first measurement. Furthermore, the release efficiency was not fully recovered in spite of the temperature rise. From these results, the sintering of the target proceeded and the target crystal structure was expected to become more dense. Therefore, the effusion time from the target became much longer. To improve this situation, the thermal stability of the crystal structure is required. For example, a carbon nanotube is one of a candidate material. More study of the target crystal structure is needed.

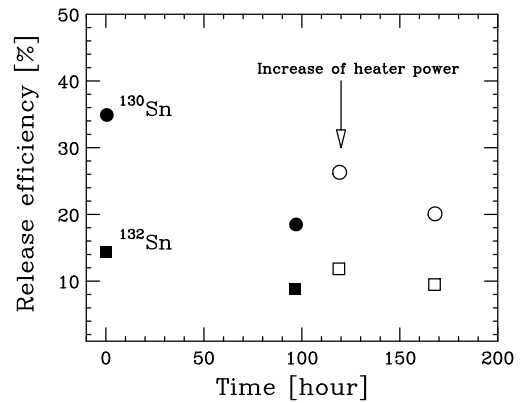


Figure 5: Time dependence of the release efficiency of ^{130}Sn and ^{132}Sn . Circles and squares show the result of ^{130}Sn and ^{132}Sn , respectively. Black and white show the target heater power 4.4 and 5 kW, respectively.

CONCLUSIONS

ERIS was constructed for the production of the RI beams at the SCRIT electron scattering facility. The RI production at ERIS has been successfully performed and the development of increasing the rate of RI has been proceeded. To improve the efficiency of release from the target, the stable supply of a 1-mm uranium-carbide disk was established, and the stability of the target was examined. Further studies in ERIS are in progress to supply the stable and intense RI beam, and realize the electron scattering with short lived nuclei.

REFERENCES

- [1] T. Suda et al., Prog. Theor. Exp. Phys. 2012, 03C008 (2012), and references there in.
- [2] M. Wakasugi et al., Nucl. Instrum. Methods A 532, 216 (2004).
- [3] M. Wakasugi et al., Phys Rev. Lett. 100, 164801 (2008).
- [4] T. Suda et al., Phys Rev. Lett. 102, 102501 (2009).
- [5] M. Wakasugi et al., Nucl. Instrum. Methods B 317, 668 (2013).
- [6] T. Ohnishi et al., Nucl. Instrum. Methods B 317, 357 (2013).
- [7] Yu. Ts. Organessian et al., Nucl. Phys. A 701, 87c (2002).
- [8] S. Sundell et al., Nucl. Instrum. Methods B 70, 160 (1992), and references there in.
- [9] G. D. Alton, Nucl. Instrum. Methods A 382, 207 (1996), and references there in.
- [10] M. Giaeri, ENDF/BB MT-18, NNDC and H. Reis et al., Phys. Rev. C 29, 2346 (1984).
- [11] D. De Frenne et al., Phys. Rev. C 29, 1908 (1984).
- [12] Gmelin handbook of inorganic chemistry, Supplement Volume C12.
- [13] M. Cheikh Mhamed et. al., Nucl. Instr. Meth. B 266, 4092 (2008).